in the noncentrosymmetric trigonal Se and Te structures. We have not attempted to predict the magnitude of the intensity differences. To determine whether these differences are measurable would require a knowledge of the form of the radial functions R_{pl} and an estimate of the electron-population coefficients for these structures.

Chandrasekaran (1968) has also suggested that Bijvoet intensity differences may be observed in the noncentrosymmetric elements. However, our arguments for their appearance are independent of Chandrasekaran's postulates.

The existence of the chain structure in trigonal Se and Te is manifested by the anisotropy ratio of intrachain to interchain bonding strength as reflected in lattice dynamic and electronic structure studies of these structures (Joannopoulos, Schlüter & Cohen, 1975; Martin, Lucovsky & Helliwell, 1976; and references therein). The atoms within each chain are tightly and covalently bonded to two neighbours; the interchain bonding is partly van der Waals in character with an admixture of some covalent bonding. This anisotropy in the bonding renders particularly desirable a more complete representation of the atomic charge density than the usual spherically symmetric representation, and gives credibility to our discussion.

As well as providing information of considerable value about bonding features, observation of Bijvoet intensity differences in noncentrosymmetric elemental structures may also aid the resolution of ambiguities in their symmetry. A possible example of such an ambiguity is the question as to whether the β-uranium structure possesses a centre of symmetry (Tucker, Senio, Thewlis & Steeple, 1956).

The author is indebted to Dr Z. Barnea for reading the manuscript and suggesting improvements, and to Miss Maria Agosto for typing it. He also gratefully acknowledges the financial support of a Commonwealth Postgraduate Research Award. The work was supported by the Australian Research Grants Committee.

References

CHANDRASEKARAN, K. S. (1968). *Acta Cryst.* A**24**, 248–249.

CHERIN, P. & UNGER, P. (1967*a*). *Inorg. Chem.* **6**, 1589–1591.

CHERIN, P. & UNGER, P. (1967*b*). *Acta Cryst.* **23**, 670–671.

DAWSON, B. (1967). *Proc. R. Soc. London Ser. A*, **298**, 255–263.

FRIEDEL, G. (1913). *C. R. Acad. Sci.* **157**, 1533–1536.

IWASAKI, H. (1974). *Acta Cryst.* A**30**, 173–176.

JOANNOPOULOS, J. D., SCHLÜTER, M. & COHEN, M. L. (1975). *Phys. Rev. Sect. B*, **11**, 2186–2199.

MCINTYRE, G. J. & BARNEA, Z. (1978). *Acta Cryst.* Submitted.

MARTIN, R. M., LUCOVSKY, G. & HELLIWELL, K. (1976). *Phys. Rev. Sect. B*, **13**, 1383–1395.

STEWART, R. F. (1973). *J. Chem. Phys.* **58**, 1668–1676.

STEWART, R. F. (1976). *Acta Cryst.* A**32**, 565–574.

TUCKER, C. W., SENIO, P., THEWLIS, J. & STEEPLE, H. (1956). *Acta Cryst.* **9**, 472–474.

UNGER, P. & CHERIN, P. (1969). *Physics of Selenium and Tellurium*, edited by W. C. COOPER, p. 223. Oxford: Pergamon Press.

Acta Cryst. (1978). A**34**, 939–946

The Crystal Structure of $4Nb_2O_5.9WO_3$ Studied by 1 MV High-Resolution Electron Microscopy

BY SHIGEO HORIUCHI, KUNITAKA MURAMATSU AND YOSHIO MATSUI

National Institute for Researches in Inorganic Materials, Sakura-mura. Niihari-gun, Ibaraki, Japan 300-31

(*Received* 3 *March* 1978; *accepted* 26 *April* 1978)

Images of pale yellow crystals of $4Nb_2O_5.9WO_3$, obtained with a 1 MV high-resolution electron microscope revealed twinned domains of a tetragonal tungsten bronze structure with a superlattice of 3 × 1 subcells. Comparison with computer calculations suggests that the cations filling the pentagonal tunnels include both Nb and W. Crystals darkened due to reduction on longer heating included no domains and were sensitive to electron irradiation; cations were knocked on from the filled to the vacant pentagonal tunnels. This suggests that some oxygens are released from the $-M-O-M-O-M-$ strings in the tunnels on reduction to weaken the chemical bonding. The number of deficient oxygens is known from the weight gain on oxidizing the crystal. Some additional experiments reveal that there is no '$6Nb_2O_5.11WO_3$' phase. The resolving power of the present microscope is discussed on the basis of the analysis of the chromatic aberration.

Introduction

It is known that over a composition range in the Nb_2O_5–WO_3 system, the crystal structures of compounds are composed of subcells of tetragonal tungsten bronze (TTB) type (Roth & Waring, 1966). $4Nb_2O_5.9WO_3$ is one of these complex compounds. The structure of the crystal was first determined by Sleight (1966). The symmetry is orthorhombic with space group $P2_12_12$, as schematically shown in Fig. 1. MO_6 octahedra share corners with adjoining ones to form TTB type subcells, where M is a cation. The unit cell consists of three TTB subcells. Four of twelve pentagonal tunnels per unit cell, indicated by dots, are occupied by $-M-O-M-O-M-$ strings parallel to the c axis. These cations occupy the sites of dodecahedral coordination. Both niobiums and tungstens are considered to be statistically distributed at these sites.

A different structure model of $4Nb_2O_5.9WO_3$ has been proposed (Craig & Stephenson, 1969). The unit cell is nearly tetragonal and consists of 3 × 3 TTB subcells, although the atomic positions are essentially the same as those in Fig. 1. The cations in the pentagonal tunnels are considered to be exclusively Nb in this case.

An observation of a $4Nb_2O_5.9WO_3$ crystal by a 100 kV electron microscope (Allpress, 1972) revealed the formation of small domains. They were mutually twinned or out-of-phase. The unit cell was composed of 3 × 1 TTB subcells in each domain. A further observation with a higher resolving power has clarified the structure of the domain boundaries (Iijima & Allpress, 1974).

These crystals were prepared in sealed capsules at a temperature near 1300°C. They sometimes appeared as different colours, due to reduction, in spite of a definite starting composition. It was not known how the structure was modified on reduction.

We are examining a series of Nb_2O_5–WO_3 complex compounds with TTB subcells by use of a high-voltage electron microscope (Hitachi 1250 type) with specially improved resolving power (Horiuchi, Matsui & Bando, 1976). In the present paper we report the results on $4Nb_2O_5.9WO_3$. Firstly, we describe the conditions of preparation of crystals with the domain structure. The modification of structure on reduction is then clarified on the basis of the *in situ* observations of atomic displacements due to electron irradiation. Since each cation site is separately imaged as a dark spot, the species of cations in the pentagonal tunnels can be defined with the aid of a computer simulation of image contrast, in which the effect not only of the spherical but also of chromatic aberration is taken into account. Some additional experiments were performed on '$6Nb_2O_5.11WO_3$'.

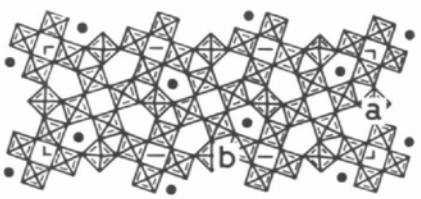

Fig. 1. Structure model of $4Nb_2O_5.9WO_3$, projected along the c axis (Sleight, 1966). The unit cell consists of 3 × 1 TTB type subcells. $a = 12{\cdot}3$, $b = 36{\cdot}6$ and $c = 3{\cdot}94$ Å.

Experimental

Nb_2O_5 (Mitsuwa Chemicals; 99·9%) and WO_3 (Johnson Matthey Chemicals; 99·99%) powders were mixed with molar ratio of 4:9 in ethyl alcohol and

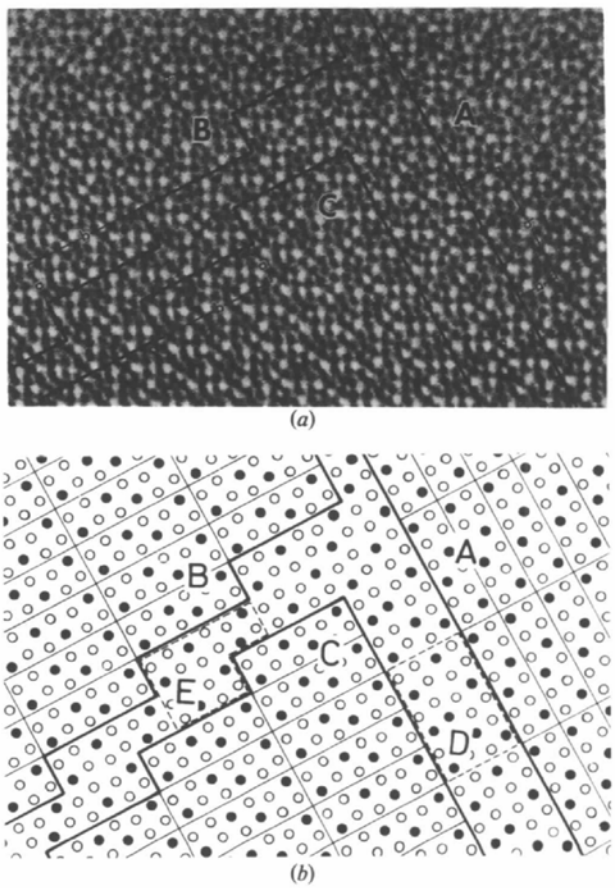

(*a*)

(*b*)

Fig. 2. 1 MV high-resolution electron microscope image of a $4Nb_2O_5.9WO_3$ crystal, prepared by heating for 20 min at 1300°C. It is composed of a number of small domains. In (*a*) dark spots represent each cation site. The unit cell is outlined. $a = 12{\cdot}3$ and $b = 36{\cdot}6$ Å. Thick lines indicate domain boundaries. Three domains, *A* to *C*, are twin-related or out-of-phase with each other. (*b*) is a schematic representation of (*a*). Open and dark circles represent the vacant and filled pentagonal tunnels, respectively.

dried. They were preliminarily maintained at 900 °C for 100 h in air. No appreciable weight change occurred during heating. They were ground in an agate mortar and closely packed in platinum capsules (15 × 4 mm ø), which were subsequently sealed. They were heated mainly at 1300 °C and quenched in iced water. The products were pale yellow. Small grains were seen to coagulate under an optical microscope. The peak profiles on the powder X-ray diffractometer chart were the same as those reported for $4Nb_2O_5.9WO_3$ (Roth & Waring, 1966). The lattice parameters are $a = 12{\cdot}3, b = 36{\cdot}6$ and $c = 3{\cdot}94$ Å. A small fraction of the crystals had a needle-like shape. The needles were thinner than 0·5 μm in diameter after heating for 20 min. The fraction of needles and their size both increased with heating time, they were about 0·8 μm in diameter and 5 μm in length after heating for 24 h.

After longer heating the colour of the crystals changed from pale yellow to black *via* grey, owing to reduction. The black crystals had a needle shape and grew much larger than those which had not darkened; for example, the diameter was about 0·1 mm on heating for 45 h. They showed a high electrical conductivity. The rate of the reduction depended on how closely the powders had been packed in the capsules before preliminary heating; when loosely packed, the darkening proceeded rapidly and black crystals were obtained within a few hours at 1300 °C or within several tens of hours at 1250 °C.

These crystals were lightly crushed and the fragments were observed through the high-voltage electron microscope operated at 1 MV. The adjustment and operation of the microscope were the same as reported previously (Horiuchi, Kikuchi & Goto, 1977). The images of the very thin crystals taken between 500 and 1000 Å underfocus could be interpreted intuitively. This is supported by the result of the computer simulation of image contrast mentioned later.

Results and interpretation

Fig. 2(*a*) is an electron microscope image of a small grain with undefined shape, prepared by heating for 20 min at 1300 °C. The crystal is composed of domains of a few hundred ångströms in size. The electron beam is incident normal to the (001) plane. The area in the figure is divided into three domains *A*, *B* and *C*. It is clear on comparing with the structure model in Fig. 1 that the dark spots in each domain correspond to the individual cation sites. The vacant pentagonal and square tunnels are seen as bright spots and even the triangular ones are resolved with intermediate contrast. Because the resolving power is better than that of any 100 kV electron microscopes, it is possible to identify the cation species occupying the pentagonal tunnels according to the contrast of the dark spots, as will be shown later with aid of computer simulation. The crystal in the domain *A* is twin-related by the mirror on the (130) plane to those in the domains *B* and *C*. In the latter two domains the crystals are out-of-phase by $\frac{1}{3}\mathbf{b}$ to each other.

At the boundary between the domains the TTB-type host lattice is formed coherently with that within the domains. The difference is in how the pentagonal

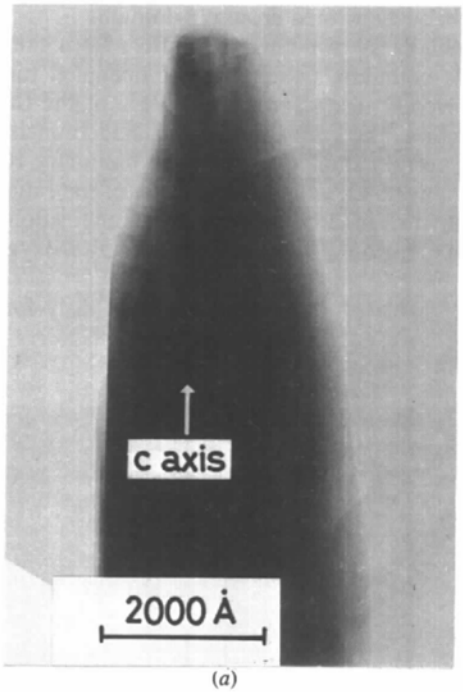

(*a*)

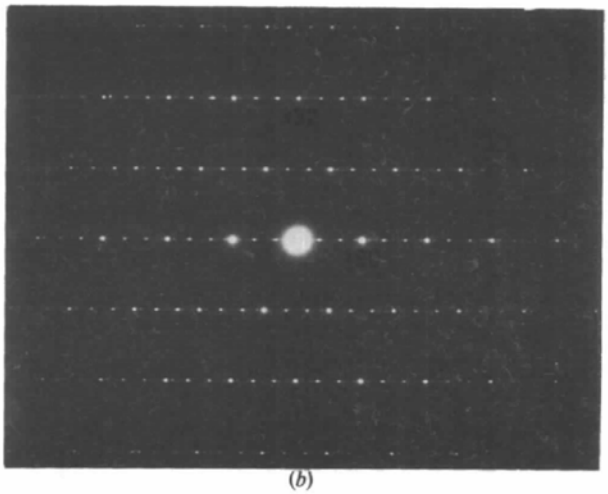

(*b*)

Fig. 3. (*a*) An image of a thin needle crystal prepared on heating for 20 min at 1300 °C. The contrast anomalies in lattice fringes may be due to twins of very fine rod shape. (*b*) The diffraction pattern of the crystal in (*a*). Strong spots are indexed based on the structure in Fig. 1. Weak spots trisecting them are from the twins. The streaks normal to the *c* axis are attributed to their shape.

tunnels are occupied. Fig. 2(*b*) is a schematic representation of (*a*). Vacant pentagonal tunnels are indicated by open circles, filled ones by black circles. Some periodic structures are often found at the boundary. At a part *D*, which is a repeating unit of such structures, the ratio of the occupied tunnels to the total is 0·333, while at *E* it is 0·300. Similar boundary structures have been reported using a 100 kV electron microscope (Iijima & Allpress, 1974). It is interesting to note in the present case that some different types of boundaries are simultaneously formed around a domain.

The thickness of boundaries differs from site to site. In thick boundaries the array of occupied tunnels is often severely disordered. Regardless of the thickness or structure, the ratio of the occupied tunnels to the total in certain small ranges of the boundary region is lower than 0·333, which is the value of the ratio within the domains. In other words, the composition in the boundary region deviates slightly to the oxygen-rich side.

Thin needle crystals were simultaneously formed in the same capsule. Fig. 3(*a*) shows an image of such a crystal, of which the top edge has been sharpened by cleavage on crushing. The diffraction pattern shows that the needle elongates along the *c* axis. Many contrast anomalies are seen in the lattice fringes. The diffraction spots are accompanied by distinct streaks normal to the *c* axis, as in Fig. 3(*b*). When the crystal is tilted the streaks remain almost unchanged. This means that planes of intensity normal to the *c* axis exist in reciprocal space. The strong spots can be indexed based on the structure with 3 × 1 TTB subcells, as indicated in Fig. 3(*b*), while the weak ones cannot. In order to account for the latter we must assume twinning occurs, which is described as the mirror operation on the (130) plane. The contrast anomalies in the image may reflect that the twins have a very fine rod shape. The diameter of the rods is estimated to be less than several tens of ångströms. The intensity planes normal to the *c* axis must have been caused by the twins. The very weak diffraction spots in Fig. 3(*b*) may originate from a larger supercell locally formed by the inter-

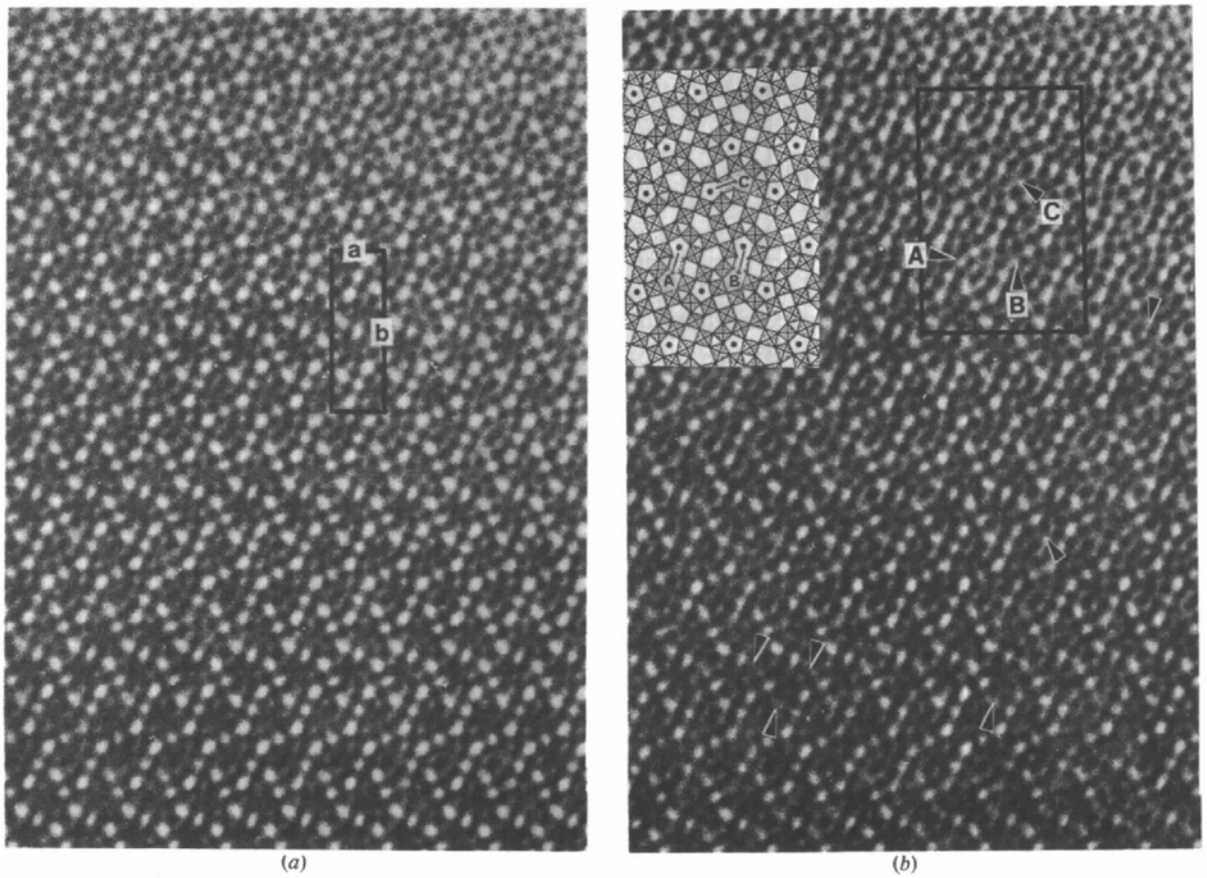

(*a*) (*b*)

Fig. 4. 1 MV high-resolution images of a reduced $4Nb_2O_5.9WO_3$ crystal. (*a*) Dark spots represent each cation site in Fig. 1. The unit cell is outlined. $a = 12{\cdot}3$ and $b = 36{\cdot}6$ Å. (*b*) The same area as (*a*) after long electron irradiation. Vacant pentagonal sites marked by arrows decrease the brightness of the spots, while adjoining filled pentagonal sites increase it. This means that the cations are knocked on by 1 MV electrons from the latter sites to the former ones, as shown schematically in the insert.

growth of the twins. No image could be observed with incident electrons parallel to the *c* axis, because no thin fragments with suitable orientation could be found.

During the crystal growth, which occurred slowly with increase of heating time, the contrast anomalies were always observed together with the streaks from the needles, so long as the crystals were not darkened.

The domains in the grain with undefined shapes also grew very slowly with heating time. Such small domains as in Fig. 2(*a*) still remained in some grains on heating for several hours at 1300 °C. The boundaries became thinner on the growth of domains.

Thin fragments were attainable from the large needle crystals which were darkened due to reduction. The image of Fig. 4(*a*) was taken from a reduced crystal heated for 45 h at 1300 °C. Neither twins nor domains were found. The contrast can be related directly to the structure model in Fig. 1. In the thin areas a dark spot corresponds to each cation site.

A remarkable difference between the reduced and unreduced crystals is noticed when they are observed for a long time in the HVEM. The former clearly changes in structure because of irradiation damage, while the latter does not. Fig. 4(*b*) is an image of the same area as (*a*) after irradiation for about 20 min. The sites of some vacant pentagonal tunnels, marked by arrows, decrease in brightness while the sites of filled tunnels near them become brighter. The contrast of the octahedral cations and of the square tunnels is not changed substantially. This indicates that the TTB host lattice remains unchanged, while some cations in the filled tunnels are shifted to neighbouring, vacant tunnel sites. The situation is schematically represented in the insert for the area outlined in Fig. 4(*b*); the initially vacant pentagonal sites like *A*, *B* and *C* are partially filled by the shifted cations.

The displacements of the cations on irradiation often occur collectively in small areas. They occur more frequently in the thicker part of the crystal. No rules were found for the direction of the displacements. No such change was observed in a 100 kV electron microscope. Thus it may be concluded that the irradiation damage is due to the knock-on of the cations by the 1 MV electrons. The temperature rise at the irradiated region may play a minor role in the present case, serving to promote the knock-on.

The knock-on occurs more frequently in the thicker part of crystal because there are more atoms. It is however difficult to estimate the exact number of knocked-on cations from the image since the intensity changes non-linearly with atom number as the thickness increases. Once some cations are displaced, the crystal lattice is locally distorted. The lattice distortion might promote the successive knock-on in this region. This may be the reason why the damage occurred collectively in small areas.

It is important to note that the cations are preferentially shifted from sites not of octahedral but of dodecahedral coordination. This means that the chemical bonding in the pentagonal site is somewhat weaker in the reduced state than in the unreduced state. A possible explanation is that some oxygens are released from the $-M-O-M-O-M-$ strings in the pentagonal tunnels during the reduction to make the cations unstable. Some of the residual oxygens must be knocked on by the electron irradiation, although they have little effect on the contrast.

In order to estimate the amount of oxygen deficiency the reduced crystals were reheated in air at 900 °C. They became transparent with a light brown colour within 3 h and the weight simultaneously increased owing to oxidation. Both the colour and weight showed no appreciable change on further heating. The ratio of the weight before and after the reheating was 0·9984. It is calculated from this value that 1·2 oxygens per unit cell are deficient in the reduced crystal. The reheated crystal was electrically non-conductive. Its fragment shows an image similar to that of Fig. 4(*a*) but is insensitive to irradiation, so long as the electron beam is kept at the minimum intensity necessary for the observation.

The oxygen vacancies in the reduced state are considered to be statistically distributed in the $-M-O-M-O-M-$ strings. Such modifications of the crystal structure as this would be difficult to detect by the conventional X-ray diffraction method. The technique using the electron irradiation damage may be widely applied to crystals with similar structural modifications and this is one of the useful applications of high-resolution HVEM.

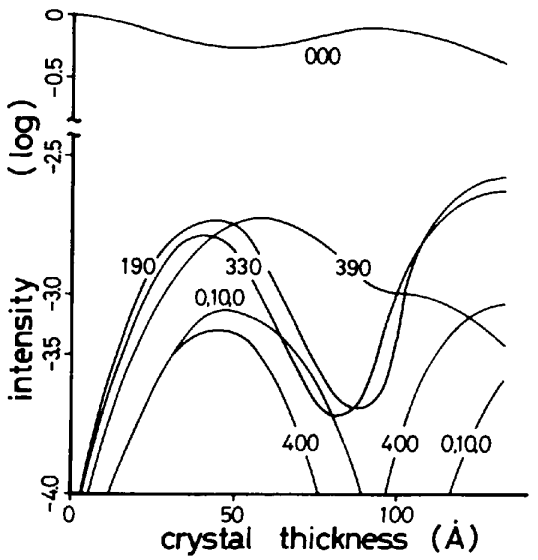

Fig. 5. Plots of calculated intensities of strongly scattered waves (with indices) against the thickness of a $4Nb_2O_5.9WO_3$ crystal, in which incident electrons are parallel to the *c* axis.

Computer simulation of images

Amplitudes of scattered waves from a $4Nb_2O_5.9WO_3$ crystal were calculated by the multislice method (Cowley & Moodie, 1957). The procedure of the calculation was as described previously (Horiuchi, Kawada, Nakano-Onoda, Kato, Matsui, Nagata & Nakahira, 1976). The dynamical interactions of 1500 waves were taken into account. Fig. 5 shows, as a result of the calculation, the intensities of some strongly scattered waves *vs* the thickness of the crystal, in which incident electrons are parallel to the *c* axis. It is assumed that Nb and W are statistically distributed at the cation sites in the pentagonal tunnels. Neutral-atom form factors (Heidenreich, 1964) were used in the calculation. The effect of absorption was neglected. It is noted that there is a shallow intensity minimum for the 000 beam at a thickness of about 50 Å.

Simulation images were computed using the following experimental values; the spherical aberration coefficient of the objective lens, $C_s = 10$ mm, the wavelength of electrons, $\lambda = 0{\cdot}0087$ Å and the radius of the objective aperture in reciprocal space, $r_{ap} = 0{\cdot}60$ Å^{-1}. The effect of chromatic aberration was taken into account after Fejes (1977), who approximated the fluctuation of the focal length by a Gaussian distribution with a standard deviation Δ. The value of Δ was changed from 0 to 600 Å at intervals of 50 Å. The calculated images were in best agreement with the real ones at $\Delta = 400$ Å. Almost the same result was obtained at $\Delta = 350$ Å.

Fig. 6 shows the through-focus series of images of $4Nb_2O_5.9WO_3$, prepared on heating for 20 min at 1300°C. It should be noted that the images change rather slowly with defocus compared with the case of 100 kV (Fejes, 1977). Simulation images computed at $\Delta = 400$ Å for a thickness of 24 Å are inserted in the

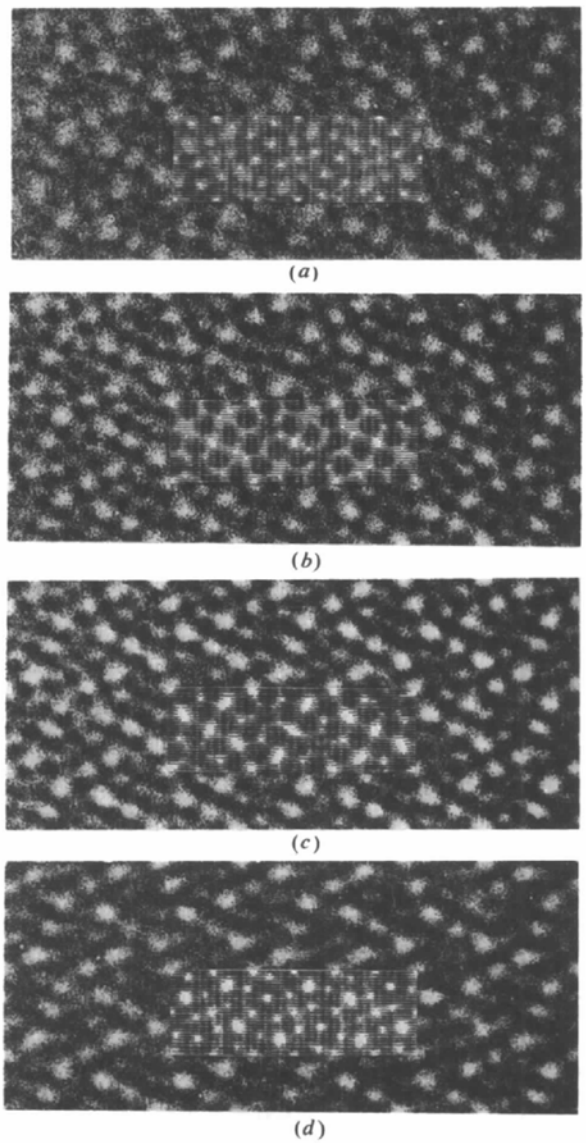

Fig. 6. Through-focus series of images of $4Nb_2O_5.9WO_3$. Computer simulation images are inserted with the same magnification. The accelerating voltage is 1 MV. The spherical aberration coefficient of the objective lens is 10 mm. The standard deviation of the focal length (Fejes, 1977) is 400 Å. The amount of underfocus is 0 (*a*), 500 (*b*), 1000 (*c*) and 1500 Å (*d*), respectively.

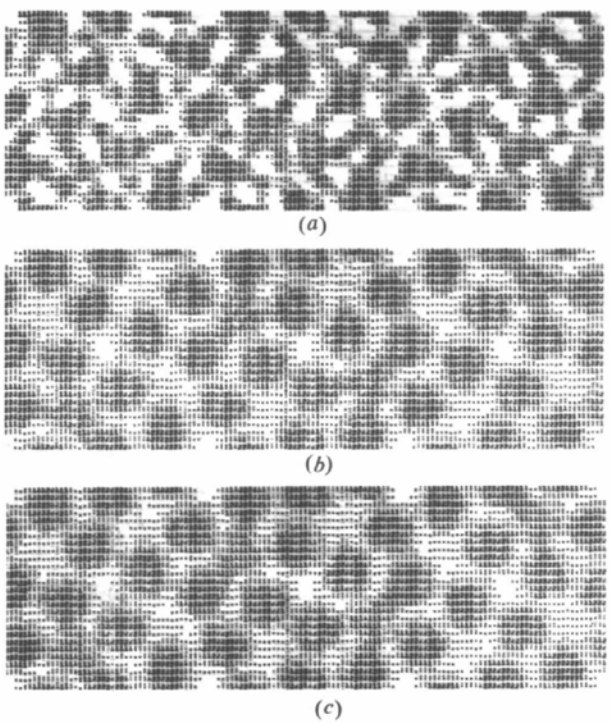

Fig. 7. Calculated images of a unit cell of $4Nb_2O_5.9WO_3$ at 500 Å underfocus. Nb and W are assumed to be statistically distributed in the pentagonal sites. $\Delta = 0$ in (*a*) and $\Delta = 400$ Å in (*b*). In (*c*) the sites are occupied exclusively by Nb, $\Delta = 400$ Å. The *a* axis is vertical (upwards) and the *b* axis points to the left.

photographs with the same scale. The correspondence between the real and calculated images is fairly good, *e.g.* the observation that the structure images appear between 500 and 1000 Å underfocus is confirmed in the calculation. The observation cannot be explained by any values of Δ except near 400 Å. Fig. 7(*a*) shows an image calculated with $\Delta = 0$ Å, *i.e.* with no chromatic aberration, at 500 Å underfocus. The difference is clear on comparing this with (*b*), for which $\Delta = 400$ Å [Fig. 6(*b*)]. Similar results were obtained by calculation in the thickness range of less than 40 Å.

When the form factors of Nb^{5+} and W^{6+} (Cromer & Waber, 1965) and O^{2-} (Sanger, 1969) ions were used in the calculation, almost the same results as above were obtained.

We then assume that the cations in the pentagonal tunnels are Nb only. Since the atomic weight differs greatly between Nb and W, the contrast at the tunnels is expected to be different. The intensities of scattered waves *vs* crystal thickness curve calculated on this assumption differed slightly from those in Fig. 5. One of the simulation images calculated is as shown in Fig. 7(*c*). The darkness of the spot at the pentagonal tunnels is about 70% of that of the surrounding octahedral cations. On comparing with the real image of Fig. 6(*b*) it seems unlikely that only Nb atoms occupy the pentagonal sites. It may at least be said that both Nb and W exist in the tunnels, although their occupational probability cannot be determined exactly from the image.

Discussion

Resolution limit of the present 1 MV *electron microscope*

The analysis of the present 1 MV high-resolution images showed that $\Delta = 400$ Å. The value is about twice that obtained for a 100 kV electron microscope (Fejes, 1977). This can be attributed mainly to the fluctuation in the high voltage ($\Delta E/E$). According to the formula, $\Delta \simeq C_c \times (\Delta E/E)$, where C_c is the chromatic aberration coefficient, the value of $(\Delta E/E)$ is calculated to be $9{\cdot}1 \times 10^{-6}$ for $C_c = 4{\cdot}4$ mm. The resolution limit due to the chromatic aberration, $d_{ch} = 1{\cdot}2\ (\Delta\lambda)^{1/2}$, of the present HVEM is 2·24 Å, which is about 0·63 times that of the 100 kV electron microscope with $\Delta = 250$ Å.

Stability of the domain structure

It was found that the domains formed in the initial stage of heating. The composition in the region of the domain boundaries slightly deviated to the oxygen-rich side. The region may serve to accommodate, to some extent, the change of composition due to reduction, which occurs on continued heating. The domains are thus kept for a certain period without being destroyed. This may be a reason why the domain structures have often been found in the crystals, although they are thermodynamically unstable.

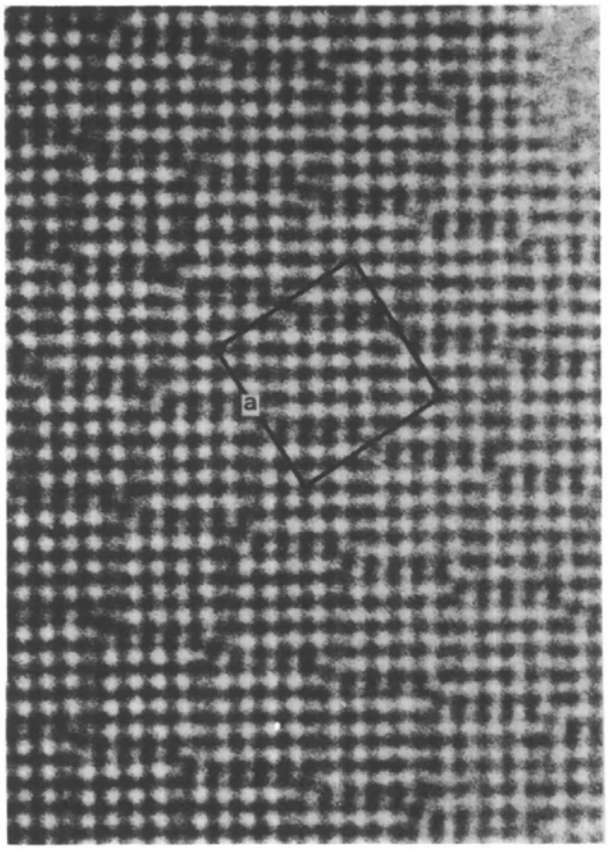

(*a*)

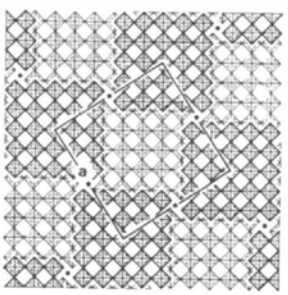

(*b*)

Fig. 8. (*a*) 1 MV high-resolution image of $9Nb_2O_5 \cdot 8WO_3$, prepared at 1250 °C. The unit cell is outlined. $a = 26{\cdot}3$ Å. In comparison with the structure model in (*b*), each cation site is resolved as a dark spot.

'$6Nb_2O_5.11WO_3$'

It was known that the powder X-ray diffractometer profile of '$6Nb_2O_5.11WO_3$' was very similar to that of $4Nb_2O_5.9WO_3$ (Roth & Waring, 1966), although a structure model has been proposed for this composition (Stephenson, 1968). Electron-microscopic observations (Iijima & Allpress, 1974; Obayashi & Anderson, 1976) could not provide any evidence of '$6Nb_2O_5.11WO_3$'. We have tried to solve the problem. Crystals with composition $6Nb_2O_5.11WO_3$ were prepared both at 1300 and 1250°C. They gave diffraction patterns and images very similar to those of $4Nb_2O_5.9WO_3$. Additional specimens with compositions $4Nb_2O_5.6WO_3$ and $5Nb_2O_5.5WO_3$ were prepared at 1300°C. It was expected from the phase diagram that the $9Nb_2O_5.8WO_3$ and $6Nb_2O_5.11WO_3$ phases coexist in both of them. The electron-microscopic observation revealed, however, the presence of $4Nb_2O_5.9WO_3$ together with $9Nb_2O_5.8WO_3$ (Roth & Wadsley, 1965). The same results were obtained from the specimens prepared at 1250°C with the same compositions, although $8Nb_2O_5.5WO_3$ and $6Nb_2O_5.11WO_3$ were expected from the phase diagram. It should be mentioned here that the reliability of the present temperature measurement is within 5°C. At any rate, it is important to note that there is no '$6Nb_2O_5.11WO_3$' phase. Fig. 8(*a*) shows a structure image of $9Nb_2O_5.8WO_3$ (tetragonal, $a = 26{\cdot}3$ and $c = 3{\cdot}81$ Å), prepared together with $4Nb_2O_5.9WO_3$ at 1250°C. It is clear on comparing with the structure model in Fig. 8(*b*) that the crystal is composed of 5×5 blocks. Each cation within the blocks is resolved as a dark spot. The cations in the octahedra sharing edges, as well as those in the sites of tetrahedral coordination, are shown in the image.

The authors wish to express their deep gratitude to Dr S. Yamaguchi, Dr Y. Bando and Mr Y. Sekikawa for their support of the present study.

References

ALLPRESS, J. G. (1972). *National Bureau of Standards Special Publication* 364, *Solid State Chemistry*, Proceedings of 5th Materials Research Symposium. Edited by R. S. ROTH & S. J. SCHNEIDER, pp. 87–111.

COWLEY, J. M. & MOODIE, A. F. (1957). *Acta Cryst.* **10**, 609–619.

CRAIG, D. C. & STEPHENSON, N. C. (1969). *Acta Cryst.* B**25**, 2071–2083.

CROMER, D. T. & WABER, J. T. (1965). *Acta Cryst.* **18**, 104–109.

FEJES, P. L. (1977). *Acta Cryst.* A**33**, 109–113.

HEIDENREICH, R. D. (1964). *Fundamentals of Transmission Electron Microscopy*, pp. 398. New York: Interscience.

HORIUCHI, S., KAWADA, I., NAKANO-ONODA, M., KATO, K., MATSUI, Y., NAGATA, F. & NAKAHIRA, M. (1976). *Acta Cryst.* A**32**, 558–565.

HORIUCHI, S., KIKUCHI, M. & GOTO, M. (1977). *Acta Cryst.* A**33**, 701–703.

HORIUCHI, S., MATSUI, Y. & BANDO, Y. (1976). *Jpn. J. Appl. Phys.* **15**, 2483–2484.

IIJIMA, S. & ALLPRESS, J. G. (1974). *Acta Cryst.* A**30**, 22–29.

OBAYASHI, H. & ANDERSON, J. S. (1976). *J. Solid State Chem.* **17**, 79–89.

SANGER, P. L. (1969). *Acta Cryst.* A**25**, 694–702.

SLEIGHT, A. W. (1966). *Acta Chem. Scand.* **20**, 1102–1112.

STEPHENSON, N. C. (1968). *Acta Cryst.* B**24**, 637–653.

ROTH, R. S. & WADSLEY, A. D. (1965). *Acta Cryst.* **19**, 38–41.

ROTH, R. S. & WARING, J. L. (1966). *J. Res. Natl Bur. Stand.* **70**A, 281–303.

Acta Cryst. (1978), A**34**, 946–949

A Simple Method for Obtaining Triclinic Cell Parameters from Weissenberg Photographs from One Crystal Setting

BY HANS HEBERT

Department of Medical Biophysics, Karolinska Institutet, S-104 01 Stockholm, Sweden

(*Received* 7 *April* 1978; *accepted* 24 *May* 1978)

A simple method is described for the interpretation of Weissenberg photographs and the determination of triclinic cell parameters from a single setting of the crystal. The theoretical approach is followed by an example illustrating the procedure. A comparison of these results with those derived from diffractometer measurements is made.